

*Submitted to Journal of Applied Crystallography*

*as a Full Article*

*Using IUCr word template version 1.3*

## **Concepts in Spin Echo Small-Angle Neutron Scattering**

*Correspondence author: Jinkui Zhao*

*Experimental Facilities Division,*

*Spallation Neutron Source,*

*Oak Ridge National Laboratory,*

*701 Scarboro Road*

*Oak Ridge, TN 37830-6474, USA*

*E-mail:zhaoj@sns.gov*

*Phone:(865) 574-0411*

*Fax:(865) 241-5177*

# Concepts in Spin Echo Small-Angle Neutron Scattering

Jinkui Zhao<sup>\*</sup>

*Spallation Neutron Source, Oak Ridge National Laboratory, Oak Ridge, TN  
37830, USA*

*E-mail: zhaoj@sns.gov*

## Synopsis

Two-dimensional spin echo small-angle neutron scattering experiments are proposed for the direct measurement of the vector-length distribution function. Interpretation of the correlation function from one-dimensional experiments is also presented.

## Abstract

Two-dimensional spin echo small-angle neutron-scattering experiments that measure the vector-length distribution function, or pair-distance distribution function, in real space are discussed. The proposed diffractometer uses two cylindrically symmetric magnetic fields with conically shaped front and end faces to enable experiments in two dimensions. It also features a  $\pi/2$  neutron spin flipper to make the effective analyzing direction of the analyzer perpendicular to the polarizing direction of the polarizer. The theoretical aspect of one-dimensional spin echo small-angle neutron-scattering experiments is also explored. The relationship between the correlation function from one-dimensional experiments and the vector-length distribution function is established, and interpretation of this correlation function in real space is presented.

## 1. Introduction

Spin echo small-angle neutron-scattering (SESANS) experiments, like the traditional spin echo method (Mezei 1972), detect changes in neutron polarization after neutrons have passed through two Larmor precession devices with opposing magnetic fields before and after the sample. In the absence of the sample, the opposite precessions of the polarization vector in the two fields cancel each other and the neutron polarization remains unchanged. In inelastic experiments, energy transfers between neutrons and the scattering sample cause the neutrons to change their speeds and hence their travel times within the second Larmor field. The net Larmor precession angle is reflected in changes of neutron polarization and is analyzed

through a polarization analyzer. In SESANS experiments, variations in neutron path lengths within the second precession field originated from sample scattering cause this net precession angle. The magnetic fields are designed with inclined entrance and exit faces (Keller et al. 1995, Rekveldt 1996) such that to the first order, the neutron path length within the Larmor device is a linear function of the scattering angle. With the development of the neutron resonance spin echo technique (Golub & Gähler 1987), it became feasible to construct Larmor precession devices with such inclined faces. The neutron resonance spin echo experiment uses a pair of spatially separated resonance spin flippers to replace the traditional magnetic field. For small-angle applications, the flippers are placed into the neutron beam at an angle, satisfying the inclination requirement (Keller et al. 1995). Many of the progresses in SESANS development have been achieved only recently. (Rekveldt 1996, 1998, 1999, & 2000; Bouwman et al. 1999 & 2000; Bouwman & Rekveldt 2000; van Oossanen et al. 2000; and Uca et al. 2000).

In a conventional small-angle neutron-scattering (SANS) experiment, the scattering intensity  $I$  is measured as a function of neutron momentum transfer  $Q$ . These  $I(Q)$ - $Q$  data are then typically transformed into real space to obtain the so-called vector-length distribution function  $p(r)$ , also called the pair-distance distribution function. A SESANS experiment, on the other hand, measures a correlation function in real space. Parallel to an inelastic spin echo experiment, where the detected time correlation function is the Fourier transform of the energy transfer spectrum, SESANS measures a correlation function that is the Fourier transform of the  $I(Q)$ - $Q$  spectrum. Rekveldt defined the following correlation function

$$G(r) = \frac{2}{p} \int S(\mathbf{Q}) \cos(\mathbf{Q} \cdot \mathbf{r}) d^2\mathbf{Q} \quad (1)$$

for the experimental setup described in (Rekveldt 1996). The  $2/p$  factor is added here for definition consistency within the current study.  $G(r)$  is obtained directly from analyzing the neutron polarization or the neutron intensity after the analyzer. In this Fourier integration, the scattering vector  $\mathbf{Q}$  is defined individually for each scattered neutron and the incoming direction of that particular neutron is the reference vector for determining  $\mathbf{Q}$ . This is contrary to conventional SANS experiments, where the incoming neutron beam direction is used to define the  $\mathbf{Q}$  vector for all scattered neutrons. The immediate implication is that the divergence of the neutron beam does not degrade the quality of the scattering data in SESANS experiments the way it does in conventional SANS experiments. In simple terms, SESANS is divergence independent. This is a key property that enables SESANS to extend its application range well into the ultrasmall-angle regime (Rekveldt 1996). Neutron beams with relatively

large divergence can thus be used to increase the counting rate. In fact, as is discussed later, divergent neutron beams are preferred not only for the increased neutron flux but also for increasing the completeness of the scattering data. Nonetheless, it must be pointed out that such divergence independence is valid only in the first-order approximation. This is because the  $G(r)$  function defined in equation (1) is valid to the first order only. Further, it must be cautioned that, depending on the instrument geometry, the divergence independence may be restricted. In the Rekveldt (1996) setup, for example, such independence is true in one direction only, namely along the direction in which scattering data are collected.

Equation (1) defines a clear relationship between the  $G(r)$  function and the scattering cross section. What  $G(r)$  represents in real space, however, is not obvious. In small-angle scattering experiments, the vector-length distribution function  $p(r)$  is most commonly used and readily interpreted. It is therefore desirable to measure the  $p(r)$  function directly from a SESANS experiment or to at least be able to interpret the  $G(r)$  function in real space. In this paper, experimental concepts where the vector-length distribution function  $p(r)$  is the directly measurable correlation function are proposed. A direct link between the  $G(r)$  and  $p(r)$  functions is also established, and the interpretation of  $G(r)$  in real space is presented.

## 2. Two-Dimensional SESANS

### 2.1 *Direct measurement of the vector-length distribution function*

The proposed SESANS setup is shown in Figure 1, with familiar components found in a typical spin echo experiment. The two key features that enable direct measurement of the vector-length distribution function are the  $\pi/2$  spin flipper and the cylindrically symmetric magnetic fields with conically shaped entrance and exit faces. To facilitate discussions, the polarizing direction of the polarizer and the analyzing direction of the analyzer are assumed to be along the x direction. In addition, the Larmor fields are assumed to be along the  $\pm z$  directions, and the  $90^\circ$  rotation of the neutron polarization by the flipper  $F_{\pi/2}$  occurs within the x-y plane. Further, only the elastic scattering is considered. For strong inelastic scattering systems, modified Larmor devices can be used to amplify the elastic contribution and suppress the inelastic contribution to the Larmor precession angle (Rekveldt 1996).

To examine the neutron intensity on the detector, neutron polarization along the pathway is followed. Immediately after the polarizer, neutrons have the polarization  $P_0$ , which is the same as the polarizing power of the polarizer. After precessing in the two opposite Larmor

fields, the polarization vector for the transmitted neutron beam remains unchanged. Consider an incoming neutron along the z axis scattered into the  $(\mathbf{q}, \mathbf{y})$  direction, the net precession angle of this neutron is (Figure 1a)

$$\Delta\mathbf{j} \approx (cIBL \cot \mathbf{q}_0)\mathbf{q}, \text{ with } c = \mathbf{g}m_N/h = 4.632 \times 10^{14} \text{T}^{-1} \text{m}^{-2}, \quad (2)$$

in the first-order approximation for the small  $\mathbf{q}$ -angle.  $\mathbf{q}$  is the scattering angle, and  $\mathbf{y}$  is the azimuthal angle.  $I$  is the neutron wavelength, and  $L$  is the length of the Larmor field  $B$  (Figure 1a).  $\mathbf{g}$  and  $m_N$  are the neutron gyromagnetic ratio and mass, respectively.  $h$  is Planck's constant.

Because of the cylindrical symmetry of the Larmor devices,  $\Delta\mathbf{j}$  does not depend on the azimuthal angle  $\mathbf{y}$ . This feature allows data collection in two dimensions, namely in the x-y plane. When compared to a one-dimensional SESANS instrument (Rekvelde 1996, see also Figure 2), the disadvantage of this two-dimensional setup is that the divergence independence is not preserved when the size of the scattering sample is not negligible. In the cross section shown in Figure 1a, the above  $\Delta\mathbf{j}$  expression is not valid for those incoming and scattered neutrons whose pathways cross the centerline (*i.e.*, the z axis) within either of the two Larmor devices. The likelihood that a neutron crosses the centerline increases with the cross section of the sample. To ensure the divergence independence, small scattering samples have to be used, which can be achieved by placing a pinhole slit just before the sample. Similar situation is found in the two alternative Larmor device configurations in Figures (1a) and (1b) and small sample slits are needed in both cases. Using small scattering samples implies immediately the loss of neutron intensity. To make up for such loss, focusing optics can be used. In principle, the use of focusing techniques on a SESANS instrument is less complicated than that on a traditional SANS instrument, because the former only needs focusing onto the sample while the latter requires focusing onto the detector.

For neutrons scattered into the  $(\mathbf{q}, \mathbf{y})$  direction, the polarization becomes  $P_0 \cos(\Delta\mathbf{j})$ . The total beam polarization is obtained by summing over all scattered and transmitted neutrons.

$$P_1 = TP_0 + P_0 \frac{1-T}{\mathbf{s}_T} \int_{4\mathbf{p}} S(\mathbf{Q}) \cos(\Delta\mathbf{j}) \sin \mathbf{q} d\mathbf{q} d\mathbf{y} ,$$

where  $S(\mathbf{Q})$ ,  $\mathbf{s}_T$ , and  $T$  are the coherent differential cross section, total cross section, and transmission of the sample, respectively.  $S(\mathbf{Q})/\mathbf{s}_T$  is the probability for a neutron to be scattered into a unit solid angle in the  $(\mathbf{q}, \mathbf{y})$  direction. For simplicity, the practical limit on the scattering angle by an actual instrument is omitted, and  $4\mathbf{p}$ -solid angle is used as the

boundary. Errors associated with a limited  $\mathbf{q}$ -range is discussed in §5. Further, the incoherent scattering cross section is not considered.

For a small  $\mathbf{q}$ , the momentum transfer  $Q = 4\mathbf{p}\sin(\mathbf{q}/2)/l \approx 2\mathbf{p}\mathbf{q}/l$ . The Larmor angle  $\Delta\mathbf{j}$  can be expressed as

$$\mathbf{Dj} = Qr \text{ with } r = \frac{1}{2\mathbf{p}} c l^2 B L \cot \mathbf{q}_0 . \quad (3)$$

The  $r$  parameter has the unit of [m]. Rekveldt (1996) described  $r$  as a length parameter of the scattering particle. Bouwman et al. (2000) stated further that  $r$  is the distance between two points or volume elements in the scattering particle. The following discussion provides a logical explanation for the  $r$  parameter.

After the  $F_{\pi/2}$  flipper, the transmitted neutrons no longer contribute to the total polarization along the x direction. Replace  $\mathbf{Dj}$  in  $P_1$  with equation (3), and add the  $90^\circ$ -phase shift to it. Also, substitute the scattering angle  $\mathbf{q}$  as well as  $\sin\mathbf{q}$  with the momentum transfer  $Q$ . The neutron polarization after the flipper becomes

$$P_2 = P_0 \frac{1-T}{2\mathbf{p}BL \cot \mathbf{q}_0 \mathbf{s}_T} \int dy \int S(\mathbf{Q}) \sin(Qr) QrdQ .$$

For isotropic scattering systems, the scattering cross section is a function of the scattering angle  $\mathbf{q}$  only and does not depend on the azimuthal angle  $\mathbf{y}$ . Cases in which ordering exists in the sample and the scattering pattern is asymmetric with regard to the  $\mathbf{y}$ -angle are not considered here. The integration over  $\mathbf{y}$  in the integral is then separated from the rest, yielding the factor  $2\mathbf{p}$

After the analyzer, the detected neutron intensity on the detector  $I(B, \mathbf{I})$  is expressed as

$$I(B, \mathbf{I}) = I_0 [1 + P_2 P_A] = I_0 \left[ 1 + \frac{1}{k} \frac{2}{B \mathbf{p}} \int S(Q) \sin(Qr) QrdQ \right] , \quad (4)$$

$$\text{with } k = \frac{2cL\mathbf{s}_T \cot \mathbf{q}_0}{\mathbf{p}P_0 P_A (1-T)} ,$$

where  $P_A$  is the analyzing power of the analyzer.  $I_0$  is the neutron intensity when  $P_2 P_A = 0$  (*e.g.*, when neutrons are totally depolarized between the polarizer and analyzer). Because of the presence of the  $F_{\pi/2}$  flipper,  $I_0$  can also be measured with the precession fields  $\pm B$  set to zero. The parameter  $k$  is a constant for a given experiment. The intensity  $I(B, \mathbf{I})$  is a function

of both the magnetic field and the neutron wavelength, which is evident explicitly, or implicitly, through the  $r$  parameter [equation (3)].

The integral part in equation (4) defines the vector-length distribution function  $p(r)$  (Guinier & Fournet 1955).

$$p(r) = \frac{2}{\pi} \int_0^\infty S(Q) \sin(Qr) (Qr) dQ \cdot \quad (5)$$

The upper integration limit for the momentum transfer is determined by the wavelength of the neutrons and the maximum scattering angle of  $180^\circ$ . For mathematical convenience, infinity is commonly used. For scattering particles with uniform scattering length density,  $p(r)$  is the distribution of the distances  $r$  joining two points or volume elements. Thus, the  $r$  parameter defined in equation (3) is the length of the scattering vector within the scattering particle. The reverse transform of equation (5), which will be used in the next section, is listed here as a reference.

$$S(Q) = \int_0^\infty p(r) \frac{\sin(Qr)}{Qr} dr \cdot \quad (6)$$

Infinity is again used as the upper limit for  $r$  for mathematical convenience. The true physical limit is the maximum linear dimension of the scattering particle.

Thus, by using a  $\pi/2$  spin flipper in combination with magnetic fields that have conical front and end faces, the vector-length distribution function  $p(r)$  is measured directly. Substitution of equation (5) into equation (4) yields

$$p(r) = kB \left[ \frac{I(B, I)}{I_0} - 1 \right] \cdot \quad (7)$$

Measurements at different  $r$  values are achieved either by changing the Larmor field  $B$  or by scanning through a neutron wavelength band. Integral structure parameters of the scattering particle, such as the forward scattering intensity and the radius of gyration, are readily obtained from the zero and second moments of the  $p(r)$  function.

In addition to making the direct measurement of the  $p(r)$  function possible, the use of the  $F_{\pi/2}$  flipper has an additional benefit of suppressing half of the transmitted neutron beam, which in turn means lower background and higher signal-to-noise ratio.

## 2.2 Without the $F_{p2}$ flipper

Although the  $F_{\pi/2}$  flipper is an essential component in the proposed instrument, it is interesting to look into situations where the flipper is absent. The polarization  $P_2$  in equation (4) is now replaced with  $P_1$ . Parallel to discussions in §2.1, the correlation function is defined as

$$\Pi(r) = \frac{2}{\mathbf{p}} \int_0^\infty S(Q) \cos(Qr) (Qr) dQ \quad (8)$$

From the neutron intensity data,  $\Pi(r)$  is obtained through

$$\Pi(r) = kB \left[ \frac{I(B, \mathbf{l})}{I_0} - (1 + TP_0 P_A) \right] \quad (9)$$

Unlike the  $p(r)$  function, the  $\Pi(r)$  function is not readily interpretable in real space. By denoting  $h(r) = \Pi(r)/r$  and  $q(r) = p(r)/r$ , it is observed that  $h(r)$  and  $q(r)$  are the real and imaginary part of the complex Fourier transform of the function  $Q \cdot S(Q)$ . In the following paragraphs, it is shown that a dispersion relation exists between the  $h(r)$  and  $q(r)$  functions and that a pair of Hilbert transforms links the two functions. Substitution of  $S(Q)$  from equation (6) into equation (8) yields

$$\begin{aligned} \Pi(r) &= \frac{2}{\mathbf{p}} \int_0^\infty p(r') \frac{r}{r'} dr' \int_0^\infty \sin(Qr') \cos(Qr) dQ \\ &= -\frac{1}{\mathbf{p}} \int_0^\infty p(r') \frac{r}{r'} dr' \left[ \frac{\cos(r' - r)Q}{r' - r} + \frac{\cos(r' + r)Q}{r' + r} \right]_{Q=0}^\infty \end{aligned}$$

Because  $p(r) = 4\mathbf{p}r^2 \mathbf{g}(r)$ ,  $\mathbf{g}(r)$  is the correlation function in small-angle scattering (Debye & Bueche 1949) and is analytic; therefore, the function  $p(r)/r$  is also analytic. The contour of integration can thus be deformed off the real axis in the complex plane of  $r' = u + iv$ . The above integral is rewritten as

$$\begin{aligned} \Pi(r) &= -\frac{1}{2\mathbf{p}} \int_{C_-} p(r') \frac{r}{r'} dr' \left[ \frac{e^{-i(r'-r)Q}}{r' - r} + \frac{e^{-i(r'+r)Q}}{r' + r} \right]_{Q=0}^\infty \\ &\quad - \frac{1}{2\mathbf{p}} \int_{C_+} p(r') \frac{r}{r'} dr' \left[ \frac{e^{i(r'-r)Q}}{r' - r} + \frac{e^{i(r'+r)Q}}{r' + r} \right]_{Q=0}^\infty \end{aligned}$$

The contour  $C_-$  is chosen below the real axis ( $v < 0$ ) for the first integral, and the contour  $C_+$  is chosen above the real axis ( $v > 0$ ) for the second integral. Replacing  $r'$  with  $u + iv$ , the exponentials are written as  $e^{\pm i(r' \pm r)Q} = e^{\mp vQ} e^{\pm i(u \pm r)Q}$ . Therefore, the choice of the contours

guarantees that all the exponentials vanish as  $Q \rightarrow \infty$ . Omitting the notion for the contours, the previous equation becomes

$$\Pi(r) = \frac{2r}{\mathbf{P}} \int_0^\infty \frac{p(r')}{r'^2 - r^2} dr' . \quad (10)$$

Similarly, the reverse transform of equation (10) is found by substituting the reverse transform of equation (8),

$$S(Q) = \int_0^\infty \Pi(r) \frac{\cos(Qr)}{Qr} dr ,$$

into equation (5). With the same procedure, it is found to be

$$p(r) = -\frac{2r^2}{\mathbf{P}} \int_0^\infty \frac{\Pi(r')}{r'(r'^2 - r^2)} dr' . \quad (11)$$

Equations (10) and (11) describe the dispersion relationship between the  $\Pi(r)$  and  $p(r)$  functions. Both of them have a singular point at  $r' = r$ . Figure 3 plots the  $p(r)$  and  $\Pi(r)$  functions for a uniform sphere. It is noted that  $\Pi(r)$  goes to negative at large  $r$ 's. It is also noted that  $\Pi(r)$  is an experimentally measurable quantity. This is not a contradiction because  $\Pi(r)$  is obtained by subtracting a constant from the actually measured  $I(B, I)$  data [equation (9)].  $I(B, I)$  is the neutron intensity or neutron counts that cannot be negative.

### 3. One-Dimensional SESANS

#### 3.1 $p(r)$ -measurement in one-dimensional experiments

When the Larmor precession devices have flat, inclined entrance and exit faces, as described in Rekveldt (1996) (see also Figure 2), the equations that have been derived for measurements in two dimensions are no longer applicable. This is because the Larmor precession angle  $\mathbf{Df}$  is now a function of the azimuthal angle  $\mathbf{y}$ . Equation (3) is replaced by

$$\Delta \mathbf{j} = Qr \cos \mathbf{y} . \quad (12)$$

The correlation function defined with this  $\Delta \mathbf{j}$  cannot be readily interpreted in real space. To obtain a meaningful correlation function, constraint on the instruments is made. From equation (12), it can be seen that if a slit is added between the sample and the detector to limit the azimuthal  $\mathbf{y}$  angle to a small range  $(-\Delta \mathbf{y}/2, \Delta \mathbf{y}/2)$  such that  $\cos \mathbf{y} \rightarrow 1$ , the formalism

presented in §2 can be used again. The only modification to the equations is to replace the constant  $k$  in equations (7) and (9) with  $k' = (2\mathbf{p}/\Delta\mathbf{y})k$ .

To maintain a constant  $\Delta\mathbf{y}$  range for all scattering angles  $\mathbf{q}$ , the slit has to have the shape of a sand clock (Figure 2). Parallel to discussions in §2.1, the size of the sample has to be small for  $\cos\mathbf{y} \rightarrow 1$  to be valid for all neutrons scattered off the sample. The loss in neutron counting rate on the detector due to small sample can at least be partially compensated by the usage of focusing optics.

### 3.2 Rectangular slit, no $F_{\pi/2}$ flipper - Rekveldt setup

With a rectangular slit along the  $x$  direction (Figure 2), the discussion in §3.1 is no longer applicable because the range of the azimuthal angle  $\Delta\mathbf{y}$  is now inversely proportional to the scattering angle  $\mathbf{q}$ . Assuming the scattering sample has a negligible dimension in the  $y$  direction, a one-dimensional approximation along the slit direction (*i.e.*, the  $x$  direction) can be used. Rekveldt (1996) uses supermirrors aligned close to the  $x$ - $z$  plane as the analyzer. The limited total reflection angle of the mirrors restricts the acceptable  $Q$ -range along the  $y$  direction ( $\Delta Q_y$ ). In the following discussions, such a  $Q$  limitation is approximated as an effective narrow slit. Errors associated with a finite  $\Delta Q_y$  value are discussed as well.

To have the same configuration as in Rekveldt (1996), the  $\mathbf{p}2$  spin flipper is removed from the neutron beam path. The importance of the Rekveldt setup is underlined by recent technical developments (Bouwman et al. 1999 & 2000).

In one-dimensional approximation, the correlation function in equation (1) is modified to

$$G(r) = \frac{2}{\mathbf{p}} \int_0^{\infty} S(Q) \cos(Qr) dQ \cdot \quad (13)$$

The integration is taken along the  $+x$  direction only. Integration along  $-x$  direction defines the same  $G(r)$ . For reference, the inverse transform of equation (13) is given by

$$S(Q) = \int_0^{\infty} G(r) \cos(Qr) dr \cdot \quad (14)$$

From neutron intensity on the detector  $I(\mathbf{B}, \mathbf{I})$ ,  $G(r)$  is obtained through [compare to equation (9)]

$$G(r) = \frac{k''}{\mathbf{I} \Delta \mathbf{q}_y} \left[ \frac{I(\mathbf{B}, \mathbf{I})}{I_0} - (1 + f_2 TP_0 P_A) \right] \cdot \quad (15)$$

The constant  $k''$  is defined as  $k'' = \frac{2\mathbf{s}_T}{f_1(1-T)P_0P_A}$ .  $f_1$  and  $f_2$  denote the fractions of scattered and transmitted neutrons that pass the slit, respectively.  $\Delta\mathbf{q}_y$  is the maximum scattering angle along the y direction accepted by the slit or the supermirror. The wavelength factor  $\mathbf{I}$  comes from the substitution of integration over solid angle with integration over  $Q$  in  $G(r)$  [equation (13)]. On steady state neutron sources, where the scanning in  $r$  space is commonly achieved by changing the magnetic field [equation (3)], both  $\Delta\mathbf{q}_y$  and  $\mathbf{I}$  remain unchanged. The extraction of the  $G(r)$  function from the experimental data [equation (15)] is then straightforward. On time of flight instruments where wavelength changes, the situation is different. With a rectangular slit, the  $\Delta\mathbf{q}_y$  value remains unchanged for a given experiment. Therefore, only a  $\lambda^{-1}$ -correction is needed when extracting  $G(r)$  from the scattering intensity [equation (15)]. With a supermirror analyzer,  $\Delta\mathbf{q}_y$  increases linearly with neutron wavelength, resulting into a  $\lambda^{-2}$ -correction.

Obviously, for equations (13) and (14) to be valid,  $\Delta\mathbf{q}_y$  and its corresponding  $Q$ -range  $\Delta Q_y$  have to be small. Analog to the arguments regarding the minimum experimental  $Q$  value and the maximum scattering particle size  $D_{max}$  in traditional SANS experiments (Feigin & Svergun 1987), a good limit on  $\Delta Q_y$  would be  $\Delta Q_y < \pi/D_{max}$ . A larger  $\Delta Q_y$  will result in a smearing effect which will be discussed in detail elsewhere. In Rekveldt (1996), the total reflection angle of the supermirror analyzer is  $3 \text{ mrad}/\text{\AA}$ , which corresponds to  $\Delta Q_y \sim 0.02 \text{ \AA}^{-1}$ , or  $D_{max} \sim 150 \text{ \AA}$ . To study large particles, better limit on  $\Delta Q_y$  has been imposed, such as by using an analyzer slit in front of the analyzer. Such a slit, along with the previous assumption that the sample dimension in the y direction is negligible, reduces the neutron counting rate on the detector. To increase the counting rate, the Rekveldt setup could be modified to use a multi channel supermirror analyzer in combination with a Soller collimator (Soller 1924) in front of the analyzer, with each collimator channel defining the maximum  $\Delta Q_y$  value. Such a setup will allow the use of large samples (*i.e.*, along the y direction).

To seek an interpretation of  $G(r)$  in real space, a relationship between the  $G(r)$  and  $p(r)$  functions is established. Substitution of  $S(Q)$  in equation (13) with equation (6) leads to

$$\begin{aligned} G(r) &= \frac{2}{P} \int_0^\infty \frac{p(r')}{r'} dr' \int_0^\infty \frac{\sin(Qr') \cos(Qr)}{Q} dQ \\ &= \int_r^\infty \frac{p(r')}{r'} dr' \end{aligned} \quad (16)$$

The integral over  $Q$  in the first step vanishes for  $r' < r$  but yields  $p^4$  for  $r' = r$  and  $p^2$  for  $r' > r$ . The second step is obtained by adding an additional ( $p^4$ ) term for  $r' = r$ . The added term is to be subtracted, but it vanishes as  $dr'$  tends 0.

The  $G(r)$  function thus corresponds to the total  $r^{-1}$ -weighted probability of finding two points within the scattering particle separated by a distance of  $r$  or larger. Two properties for the  $G(r)$  function are immediately apparent.

- (a)  $G(r)$  vanishes at the maximum linear dimension of the scattering particle  $D_{max}$ .
- (b) For a scattering particle whose  $p(r)$  function is positive for all  $r$ -values,  $G(r)$  is a monotonically decreasing function.

The first property is an immediate consequence of  $p(r) \equiv 0$  beyond  $D_{max}$ . The second property holds in most scattering experiments. Exceptions are found where the contrast of the scattering particle fluctuates below and above zero, which can be found in contrast variation experiments. The varying sign of the contrast can produce negative  $p(r)$  values for certain  $r$  regions, reflected as oscillations in the  $G(r)$  function. Now, the oscillatory behaviors in  $G(r)$  presented in Bouwman & Rekveldt (2000) can easily be understood. Figure 4 shows the  $G(r)$  and  $p(r)$  curves for the single shell model used by Bouwman & Rekveldt (2000). The model has opposing contrast for the inner cavity and the outer shell, resulting in negative  $p(r)$  for  $r$ 's in the mid-range. The negativity comes from the interatomic vectors linking the shell and the cavity. It is reflected in the  $G(r)$  function as an upturn at the  $r$  values where  $p(r)$  goes to negative and as a downturn where  $p(r)$  becomes positive again.

The reverse of equation (16) is readily obtained:

$$p(r) = -\frac{dG(r)}{dr} r \quad (17)$$

Integral structure parameters of the scattering particle can be calculated either from the hereby-obtained vector-length distribution function  $p(r)$  or directly from the  $G(r)$  function. The forward (*i.e.*, at  $Q=0$ ) scattering intensity  $I(0)$  and the radius of gyration  $R_g$  are expressed in  $G(r)$  as

$$I(0) = -\int r d[G(r)] \quad \text{and} \quad R_g^2 = \frac{1}{2} \frac{\int r^3 d[G(r)]}{\int r d[G(r)]} \quad (18)$$

$I(0)$  and  $R_g$  are thus obtained from the first and third moments of  $r$  in  $G$  space.

### 3.3 Rectangular slit, with $F_{\pi/2}$ flipper

When an  $F_{p2}$  flipper is added to the Rekveldt setup, the correlation function is defined as the sine transform of  $S(Q)$ :

$$\Gamma(r) = \frac{2}{P} \int_0^{\infty} S(Q) \sin(Qr) dQ \cdot$$

$\Gamma(r)$  is extracted from the neutron intensity data through

$$\Gamma(r) = \frac{k''}{I \Delta q_y} \left[ \frac{I(B, I)}{I_0} - 1 \right] \cdot$$

The situation becomes similar to §2.2 in terms of relating  $\Gamma(r)$  to  $G(r)$  since a dispersion relation exists between them as well. With the same procedure as in §2.2, the dispersion relation is found to be

$$\Gamma(r) = -\frac{2r}{P} \int_0^{\infty} \frac{G(r')}{r'^2 - r^2} dr' \quad , \quad \text{and} \quad G(r) = \frac{2}{P} \int_0^{\infty} \frac{r' \Gamma(r')}{r'^2 - r^2} dr' \cdot$$

Under certain circumstances, measuring  $\Gamma(r)$  could be preferred since the use of the  $F_{p2}$  flipper suppresses half of the transmitted neutron beam.

## 4. Time of flight SESANS

On a pulsed neutron source, neutrons of different wavelength are selected according to their travel times from the source to the detector. This intrinsic property of sweeping through a wavelength band means that scanning through the  $r$  space [equation (3)] is automatic. A time-of-flight SESANS instrument thus has a great advantage over instruments on steady-state sources. The speed at which neutron wavelength changes on time-of-flight instruments can be much higher than that of sweeping through a magnetic field; thus, very rapid experiments become possible. With a strong neutron source, such as the Spallation Neutron Source under construction at Oak Ridge National Laboratory in the United States, it will be possible to collect a whole  $p(r)$ - $r$  or  $G(r)$ - $r$  data set with good statistics within a single neutron pulse. The instrument can be constructed and tuned such that the wavelength spectrum within a single frame covers the whole  $r$  space. This should become possible since  $r$  is a function of wavelength squared [equation (3)].

On the contrary side, special care must be taken on pulse sources in both designing the instrument and conducting an experiment. Since an instrument has fixed dimensional

parameters, the  $Q$ -range covered by the instrument changes with varying neutron wavelength. Potential truncation errors, as are discussed in more detail in the next section, will then vary with the neutron wavelength. Also, from technical discussions in the next section, broadband neutron polarizers and flippers are necessary on time-of-flight SESANS instruments.

## 5. Discussion

When properly configured and constructed, SESANS experiments can be used to measure the correlation functions that are readily interpretable in real space. In two-dimensional SESANS experiments (§2.1), the vector-length distribution function  $p(r)$  is the direct measurable quantity. In one dimension, either the  $p(r)$  or the  $G(r)$  function is directly extracted from the neutron data on the detector depending on the design of the slit (§3). In broad terms, all these functions are Fourier transforms of the scattering cross section. Thus, the accuracy of their measurements depends not only on the statistical limitations of the experiment but also on the sampling size and range in  $Q$ -space. The use of divergent neutron beams and finite neutron wavelength spread can essentially ensure that the sampling can be made fine enough. The  $Q$ -range limitation that is associated with each instrument however could lead to truncation errors in the measured correlation functions. These errors may be reflected in the form of fluctuations in the measured  $p(r)$  and  $G(r)$  functions or in that these functions do not vanish at the maximum linear dimension  $D_{max}$  of the scattering particle. For typical small-angle scattering studies,  $D_{max}$  is not a known parameter before the experiment. Reducing the truncation error is thus very important for obtaining correct structural information. The detector coverage on a SESANS instrument therefore should be as large as practically feasible. Such coverage cannot be increased without a consequence either. When the scattering angle is too large, the first-order approximation that has led to the expressions in equations (3) and (12) is no longer valid and the formalism presented here cannot be used for SESANS anymore. These limitations together restrict the smallest particle size that can be studied by SESANS. On the large-scale side, when an instrument is properly configured, the primarily limiting factors on the maximum  $D_{max}$  value that can be studied by a SESANS instrument are no longer the geometrical parameters of the instrument, as is the case in conventional SANS. Rather, they are the homogeneity and accuracy of the magnetic fields, as well as the accuracies of the polarizer and analyzer. It is reported that particles  $10^4 \text{Å}$  and larger in size can be studied (Rekveldt 2000, Bouwman et al. 2000), extending SESANS well into the ultrasmall angle regime. Detailed analysis on the SESANS resolution function is currently under way.

In general, a SESANS experiment is beam divergence independent, and for reasons just discussed, divergent beams are preferred to well-collimated ones. In a Rekveldt setup (§3.2), such independence is maintained only along the slit direction. On a two-dimensional SESANS instrument (§2) and in its one-dimensional approximation (§3.1), the beam divergence independence is maintained when the size of the scattering sample is negligible.

On the technical side, the design of a cylindrically symmetric Larmor precession device with conical ends may present some challenges. One might imagine that it should be possible to use cone-shaped mu-metals or superconductors to cover a solenoid to form such a device. Resonate spin flippers (Golub & Gähler 1987) and the recent development of magnetized foils in SESANS application (Bouwman *et al.* 2000) could also be explored for the current purpose. The conical faces of the Larmor device may also be approximated by many triangles that could lead to an easier construction.

On steady-state neutron sources, the neutron polarizer and analyzer pose no serious challenge since supermirror polarizers can be used. Supermirrors are also applicable on pulsed neutron sources when only access to long wavelength neutrons is desired, though it would be challenging in a two-dimensional SESANS experiment. To access short wavelength neutrons, alternative polarizers such as the polarized  $^3\text{He}$  spin filters (Gentile & McKeown 1993) have to be evaluated. The disadvantage of  $^3\text{He}$ -polarizers is that high neutron polarization is difficult to achieve. Another possibility is to use a dynamically polarized hydrogen target (Zhao *et al.* 1995) as the spin filter. Close to full polarization of the hydrogen can be obtained, and hence high neutron polarization can be achieved. The polarized target is, however, primarily suited as a polarizer only. Unlike polarized  $^3\text{He}$ , which has a spin-dependent cross section for neutron absorption, the filtering effect of polarized hydrogen comes from the large spin-dependent scattering cross section of the hydrogen. Neutrons with the “wrong” spin direction are scattered in a  $4\pi$  solid angle. If a polarized hydrogen target is used as an analyzer, a relatively large portion of the scattered neutrons will be detected on the detector, degrading the effectiveness of the analyzer.

Broadband spin flippers will also be needed on pulsed neutron sources. Recent progresses in the development of Drabkin flipper appear to hold great promise (Parizzi *et al.* 2000, Klose 2001).

[Figure Captions]

**Figure 1 (a)** Cross-sectional view of the proposed two-dimensional SESANS setup. The two Larmor precession devices ( $\pm B$ ) before and after the sample (O) have conical ends with rotational symmetry around the centerline of the Larmor devices (*i.e.*, the  $z$  axis). The polarizing power of the polarizer P and analyzer A are  $P_0$  and  $P_A$ , respectively. The flipper  $F_{\pi/2}$  is located before the analyzer and rotates the neutron polarization by  $90^\circ$ . The detector D is located behind the analyzer. The coordination system is defined such that the  $x$ ,  $y$ , and  $z$  axes are along the vertical, horizontal, and neutron beam directions, respectively. In this system, the scattering angle  $\mathbf{q}$  and the azimuthal angle  $\mathbf{y}$  form the conventional polar angles. The azimuthal angle  $\mathbf{y}$  is defined as the angle between the  $x$  axis and the projection of the scattering direction on the  $x$ - $y$  plane. **(b,c)** Two alternative setups with the sample centered between the two Larmor devices. The net Larmor precession angle of the neutron polarization in equation (2) becomes  $\Delta\mathbf{j} \approx \pm[cIB(L+2l)\cot\mathbf{q}_0]\mathbf{q}$ , respectively.  $l$  is the distance between the sample and either of the two Larmor devices along the  $z$  axis. In **(b)**, a divergent incoming neutron (solid line with arrow) and a scattered neutron (dashed line with arrow) are shown. The validity of the net precession angle  $\Delta\mathbf{j}$  in this case is ensured by the added small pinhole slit in front of the sample (see text). The same argument is also true for the cases **(a)** and **(c)**.

**Figure 2** Left: One-dimensional SESANS setup based on Rekveldt (1996), with the modification of an optional slit (S) and a  $\pi/2$  flipper ( $F_{\pi/2}$ ) added before the analyzer. The symbols and the coordinate system are defined as in Figure 1. Right: a sand-clock slit as viewed along the incoming neutron beam direction. Its usage is discussed in §3.1.

**Figure 3** Calculated  $p(r)$ (circles) and  $\Pi(r)$  (solid line) functions for a spherical particle with a  $1000\text{-\AA}$  radius and uniform scattering density.

**Figure 4** Calculated  $p(r)$  (circles) and  $G(r)$  (solid line) functions for a spherical shell with a 1000-Å outer radius and a 700-Å inner radius. The contrast of the shell and its inner cavity are 1 and  $-1$ , respectively.

*Acknowledgement* This work was carried out at Oak Ridge National Laboratory, which is managed by UT-Battelle, LLC, under contract DE-AC05-00OR22725 for the U.S. Department of Energy.

## References

- Bouwman, W. G., Kraan, W., and Rekveldt, M. T. (1999) *Physica B* **267-268** 79-83.
- Bouwman, W. G., van Oossanen, M., Uca, O., Kraan, W., and Rekveldt, M. T., (2000) *J. Appl. Cryst.* **33**. 767-770.
- Bouwman, W. G., and Rekveldt, M. Th. (2000) *Physica B* **276-278** 126-127.
- Debye, P., and Bueche, A. M. J. (1949) *J. Appl. Phys.* **20**, 518-525.
- Feigin, L. A., and Svergun D. I. (1987) *Structure Analysis by Small-Angle X-Ray and Neutron Scattering* and references therein.
- Gentile, T. R., and McKeown, R. D. (1993) *Phys. Rev. A* **47** 456-467.
- Golub, R., and Gähler, R. (1987) *Physics Lett. A.* **123**, 43-48.
- Guinier, A., and Fournet, G. (1955) *Small angle Scattering of X-ray*, Wiley, New York.
- Keller, T., Gähler, R., Kunze, H., and Golub, R. (1995) *Neutron News.* **6** no.3. 16-17.
- Klose F. (2001) Personal communication.
- Mezei, F. (1972) *Z. Phys.* **255**, 146-160.
- Parizzi, A. A., Felcher, G. P., and Klose F. (2000) *Proceedings of the 15<sup>th</sup> Meeting of the International Collaboration on Advanced Neutron Sources* In press.
- Rekveldt, M. T. (1996) *Nucl. Instr. & Math. in Phys. Res. B*, **114**, 366-370.
- Rekveldt, M. T. (1998) *J. Appl Phys.* **84**, no 1. 31-37.
- Rekveldt, M. T. (1999) *PNCMI 98, Physica B* **267-268** 60-68.
- Rekveldt, M. T. (2000) *Physica B* **276-278**. 55-58.
- Soller, W., (1924) *Phys. Rev.* **24** 158.
- van Oossanen, M., Kraan, W. H., Bouwman, W. G., and Rekveldt, M. T. *Physica* (2000) *B* **276-278**. 134-135.
- Uca, O., Bouwman, W. G., Kraan, W. H. and Rekveldt, M. T. (2000) *Physica B* **276-278**. 136-137.
- Zhao, J., Meerwinck, W., Niinikoski, T., Rijllart, A., Schimitt, M., Willumeit, R., and Stuhmann, H. (1995) *NIM A* **356**. 133-137.

[Figure 1]

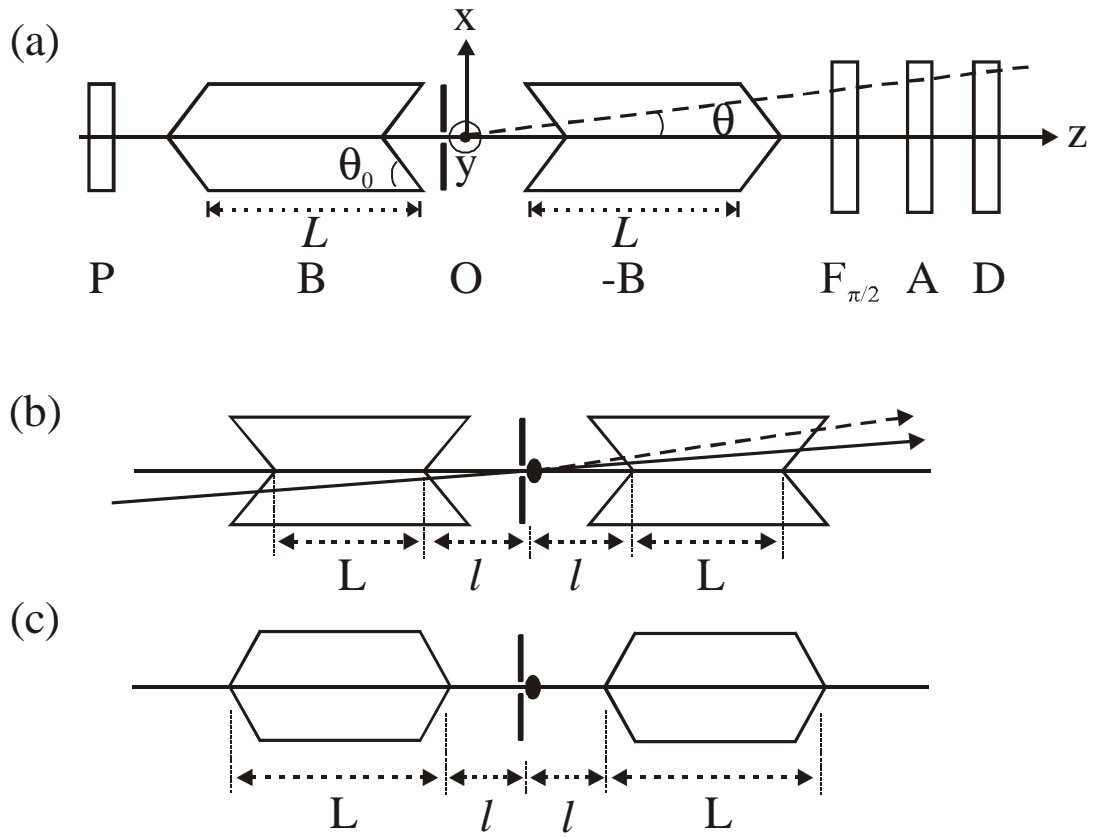


[Figure 2]

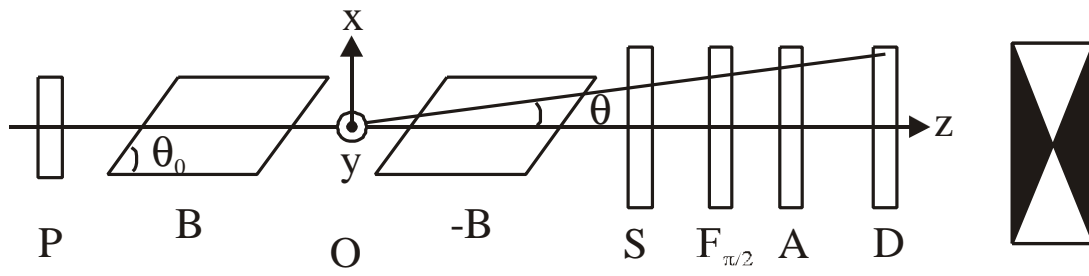


[Figure 3]

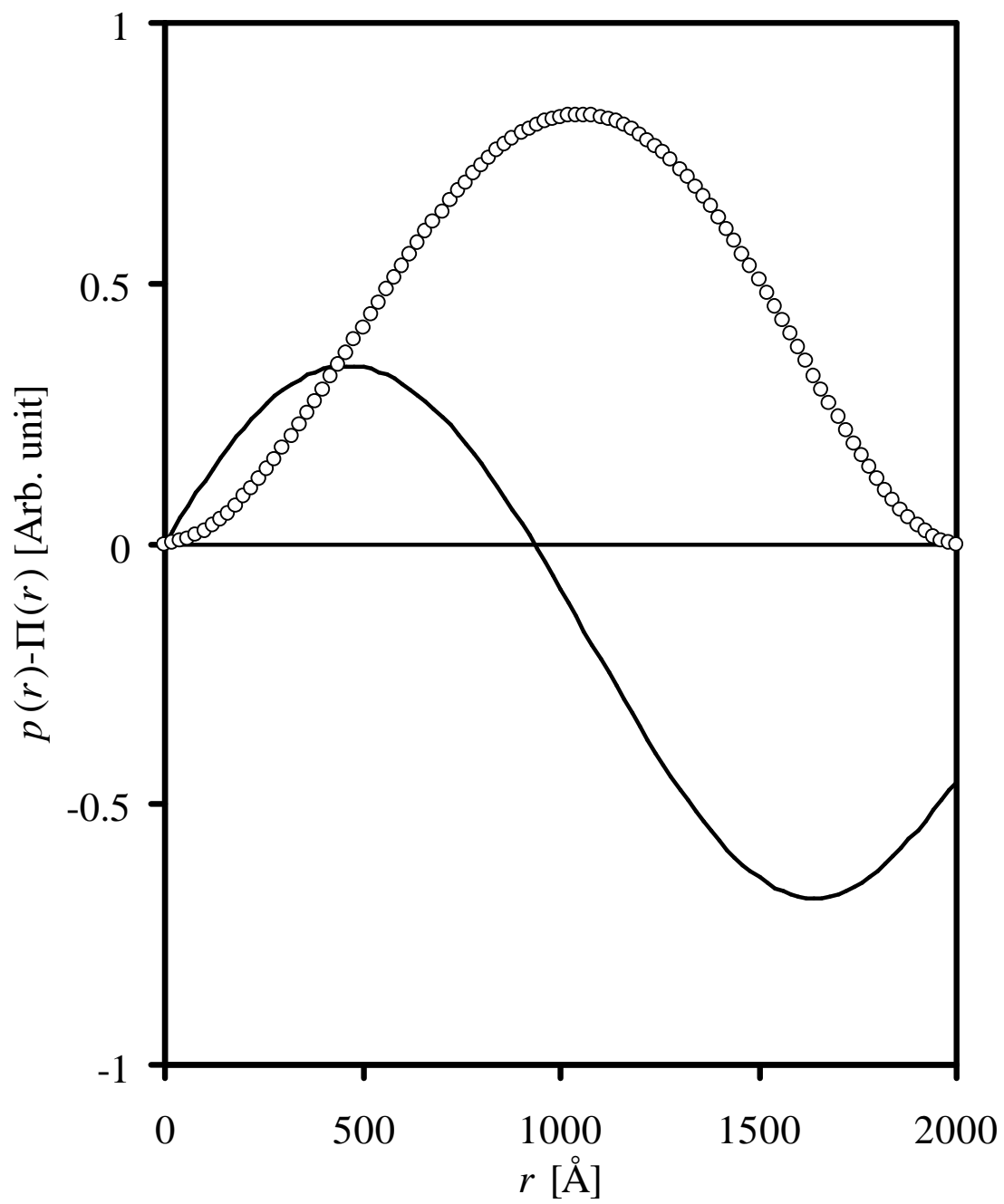


[Figure 4]

